THE JOURNAL OF PHYSICAL CHEMISTRY B

ARTICLE

pubs.acs.org/JPCB

Dynamic Structure Factor for Large Aggregate Clusters with Internal Motions: A Self-Consistent Light-Scattering Study on Conjugated Polymer Solutions

Yu H. Wen,[†] Po C. Lin,[†] Chi C. Hua,*[,†] and Show A. Chen[‡]

[†]Department of Chemical Engineering, National Chung Cheng University, Chiayi 621, Taiwan, R.O.C.

[‡]Department of Chemical Engineering, National Tsing Hua University, Hsinchu 300, Taiwan, R.O.C.

ABSTRACT: The aggregation properties of a standard conjugated polymer, poly(2-methoxy-5-(2′-ethylhexyloxy)-1,4-phenylenevinylene) (MEH-PPV), in two distinct solvents (chloroform and toluene) and a range of polymer concentrations (c = 0.1−3 mg/mL) have been unequivocally resolved using combined dynamic and static light scatterings (DLS/SLS). The prime challenges for analyzing this peculiar, practically important, solution system arise from the wide size distribution and unknown aggregate morphology, as well as pronounced interferences between translational and internal motions of aggregate clusters of considerably varying size. To cope with these central difficulties, we propose a self-consistent formulation for analyzing the dynamic structure factor in DLS experiment by extending an existing theory on free-draining bead−spring chains that explicitly accounts for internal fluctuations, along with two candidate form factors on Gaussian coil and rigid sphere, respectively, serving as two limiting cases to be discriminated in combined DLS and SLS measurements. Given that no accessibility to ultrasmall angular resolutions is a prerequisite, the suggested protocol can readily be carried out in conventional light-scattering apparatus. The present analyses unanimously support the *rigid-sphere* form factor in describing the entire set of light-scattering data on MEH-PPV solutions, differing from early small-angle neutron/X-ray scattering interpretations suggesting certain 2D fractal structures for the aggregation network. Scrutiny into the interior dynamics of aggregate clusters further disclosed that the segmental motions are noticeably more suppressed than for usual, nonaggregated polymer solutions, and no existing theories based on the bead−spring picture can yet capture the observed scaling behavior as manifested by the present data. Accordingly, we report several first-revealed properties of MEH-PPV solutions on the aggregate morphology, the size distribution (and mean size), mean aggregation number, and interior segmental dynamics, which serve as valuable information for linking solution properties with those for dried thin films in contemporary applications with conducting conjugated polymers.

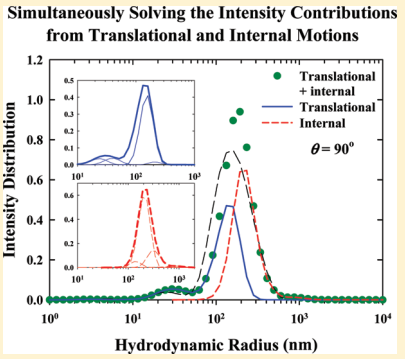

1. INTRODUCTION

Conducting conjugated polymers have nowadays become an essential solution-processable molecular material for fabricating polymer light-emitting diodes (PLEDs)[1−3] and plastic solar cells.[4,5] In addition to the possibility of producing large-area thin films at room temperature, an appealing feature of exploiting polymer semiconductors lies in the capability to fine-tune the optoelectronic properties of solution-cast thin films by using different solvents and/or polymer concentrations. Because of the semiflexible and amphiphilic attributes of most practically used conjugated polymers, however, interchain aggregates prevail in essentially all solvents even at large dilution, and their impacts on the optoelectronic properties of a solution-cast thin film are often referred to, empirically, as the memory effect.[6] Our current knowledge on the bulk aggregation state in solution has been limited, though, in part by the fact that this essential material property cannot be readily probed by spectroscopic analyses or small-angle neutron/X-ray scattering, which have commonly been employed to characterize *localized* aggregate properties in solution or in dried thin film.[7−15] As a result, no literature reports to date have embedded a comprehensive characterization of the solution properties of a conjugated polymer while taking into account a generally wide size distribution of the aggregate species whose structural features remain largely unidentified. Thus, of scientific and technological importance is to be able to unequivocally resolve the ways the aggregation properties depend on the solvent and polymer concentration used, and in practice to circumvent the major challenges as have been faced by conventional experimental measurements and analyzing schemes. Considering a widely studied conjugated polymer, poly(2-methoxy-5-(2′-ethylhexyloxy)-1,4-phenylenevinylene) (MEH-PPV), dissolved in two distinct solvents (i.e., chloroform or toluene) for a range of concentrations (i.e., c = 0.1−3 mg/mL) in the dilute regime, we address in this work how the bulk aggregation feature may be tackled unambiguously with dedicated light scattering

Received: August 31, 2011
Revised: October 25, 2011
Published: November 02, 2011

analyses. A sketch showing the molecular structure of MEH-PPV can be found in Figure 1.

It is worth mentioning that for conventional light-scattering apparatus not specially fashioned to allow access to ultrasmall-angle resolutions, the prime challenge would be that large aggregate species cannot be readily resolved from the apparent modes distribution, due to the interferences of internal segmental motions in essentially the full angular range in dynamic light scattering (DLS) experiments. Furthermore, without a priori knowledge of the morphological features of bulk aggregate species, the analyzing schemes for both dynamic and static light scattering (SLS) measurements need to be so maneuvered as to reduce the degree of ambiguity in data interpretation. This task becomes even challenging when there is a wide size distribution of the aggregate clusters, as is typically the case with standard conjugated polymer solutions. Keeping these essential features in mind, we propose a self-consistent formulation for analyzing DLS data that represents a plausible extension of an existing theory on free-draining bead−spring chains for dynamic structure factor, in conjunction with two candidate form factors for Gaussian coil and rigid sphere, respectively, to be further discriminated in SLS experiment. An important feature of this new formulation is that it requires no accessibility to ultrasmall angular resolutions and, therefore, may be carried out in conventional light-scattering apparatus. In this way, we show that it is possible to extract unequivocal information about the morphological feature, the size distribution (and mean size), mean aggregation number, and interior segmental dynamics of typical MEH-PPV solutions, which remained largely unexplored to date, yet is valuable to contemporary applications with conducting conjugated polymers. Below, we brief essential background of the conjugated polymer solutions under investigation.

In past researches, combined dynamic and static light scattering analyses have long served as a powerful means to resolve single-chain and aggregation properties for a wide range of complex solutions, including thermosensitive polymers,[16−20] rigid polymers,[21] end-capped flexible polymers,[22] copolymers,[23−26] celluloses,[27] polyelectrolytes,[28,29] microgels,[30,31] particles,[32−34] and low molar mass compounds.[35−37] In comparison, conjugated polymer solution is unique in that interchain aggregates are bolstered primarily by isotropic, weakly attractive van der Waals segmental interactions. These aggregates prevail even at large dilution, often bear a wide size distribution, and display notable nonequilibrium features upon prolonged storage that, altogether, make their comprehensive characterizations a challenging task. Moreover, differing from early studies[38−44] where the polymer species are nearly monodisperse so that the center-of-mass diffusion and internal motions can well be separated or distinguished at ultrasmall angles, the present study deals with a wide size distribution, and in particular, highly mixed chain dynamics must be resolved requiring only readily accessible range of angular detections (e.g., $30° \leq \theta \leq 150°$).

In the following text, section 2 describes essential experimental details as well as a formulation dedicated especially to tackling DLS data on a widely polydisperse solution system, where one requires simultaneously solving the contributions from translational and internal motions of widely polydisperse aggregate species. Section 3 discusses the experimental results and theoretical analyses, which lead to some first-revealed properties of MEH-PPV solutions as summarized in the same section, and the concluding remarks are given in section 4.

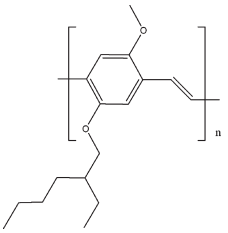

Figure 1. Sketch of the molecular structure of MEH-PPV.

2. EXPERIMENTAL SECTION

2.1. Materials and Solution Preparation. The MEH-PPV sample used in this study was purchased from Aldrich Chemical Co. and has a reported number-average molecular weight 70 000−100 000 g/mol and a polydispersity index about 5. Two representative solvents, toluene and chloroform (Mallinckrodt Chemicals, Inc.), were first filtered with a 0.22 μm PVDF Millipore filter to remove dust. All the vials used were cleaned by chloroform, followed by filtered DI water. Afterward, sample solutions with polymer concentrations 0.03, 0.1, 0.3, 1, and 3 mg/mL were prepared. During sample preparation, the solutions were sonicated 10 h per day at 50 °C (with the aid of an external water circulation system) for 4 days and stored in dark, autodry-box at room temperature. To avoid possible inhomogeneities during the sonication, we changed the position of sample solutions in the sonicator every 3 h. Prior to light-scattering measurements for fresh sample solutions, each solution was further filtered into dust-free vials using a 0.45 μm PVDF Millipore filter. The solutions were then kept stationary for 12 h to minimize the effect of perturbations due to filtration. The actual weights of MEH-PPV and solvent were redetermined for each sample solution, and the concentrations thus determined, close to the target ones, were used in later data analyses. All light-scattering measurements were conducted at 25 ± 0.1 °C.

2.2. Light-Scattering Apparatus. Light-scattering measurements were performed on a laboratory-built apparatus. The light source is a 34 mW polarized He−Ne laser emitting at 632.8 nm (Lasos, LGK 7626 S), which is beyond the absorption spectrum of MEH-PPV in the solvents used. The incident light beam was vertically polarized with respect to the light-scattering plane and focused on the sample. The cylindrical scattering cell with an inner diameter 2.1 cm (Hellma, 540.115) was thermostated to be 25 ± 0.1 °C using a Peltier thermal controller. A rotation stage with a detection arm enables the collection of scattered light in an angular range of θ = 30°−150°. The detector is a photon-counting photomultiplier tube (Hamamatsu, H7155) linked to a counting board (Hamamatsu, M9003).

The apparatus in each experimental run was first calibrated by measuring the average light intensities of toluene until the measured intensity at each angle satisfies the theoretical relation $1/\sin\theta$ within ±2%. In depolarized dynamic light scattering (DDLS) experiments, an analyzer with its transmission axis crossed to that of the polarizer was placed in front of the photomultiplier tube. To ensure the VH geometry, we manually rotated the analyzer and monitored the scattering intensity of a 7 nm radius silica colloidal dispersion until a minimum intensity was observed at each angle. Afterward, the apparatus was further confirmed to be capable of correctly producing the signals of depolarized light from a VH-active ellipsoidal α-Fe_2O_3 colloidal dispersion with known geometric properties.

2.3. Dynamic Light Scattering. The quantity measured in a homodyne light scattering instrument was the normalized intensity autocorrelation function $g^{(2)}(q,t)$, which is related to the normalized field autocorrelation function $|g^{(1)}(q,t)|$ by the Siegert relation $g^{(2)}(q,t) = 1 + \beta|g^{(1)}(q,t)|^2$,[45,46] where β ($0 < \beta < 1$) is the spatial coherence factor depending on the detection optics[47] and $q = (4\pi n/\lambda_0)\sin(\theta/2)$ is the scattering vector with n being the refractive index of the dispersion medium and λ_0 the wavelength of the incident light in vacuum. For a dilute, noninteracting, polydisperse solution system, $|g^{(1)}(q,t)|$ may be cast into a form as

$$|g^{(1)}(q,t)| = \frac{\int_0^\infty G_i(R_h)|g^{(1)}(q,t,x)|\,dR_h}{\int_0^\infty G_i(R_h)\,dR_h} \quad (1)$$

where $G_i(R_h)$ is the intensity-weighted distribution of the hydrodynamic radius. Within a free-draining bead−spring model (i.e., without hydrodynamic interaction), Pecora has derived dynamic structure factor that takes into account the translational diffusion as well as the internal motions (i.e., intramolecular relaxation) for a monodisperse system:[48] $|g^{(1)}(q,t,x)| = e^{-D_G q^2 t}\sum_{N=0}^{\infty}P_N(t,x)$, where D_G is the translational diffusivity of the polymer chain and $x = q^2R_g^2$ with R_g being the radius of gyration. In this formula, the zeroth-order $P_0(x)$ is the only term contributing to pure translational motion, and the second-order $P_2(x)$, for instance, is the first appreciable term resulting from the intramolecular relaxation within the range of $1 \le x \le 4$.

Two essential physical traits are evident in Pecora's formulation above. First, all the high-order terms of P_N are coupled with the center-of-mass diffusivity through the prefactor bearing a D_Gq^2 dependence. Second, only for data collected at ultrasmall angles or $qR_g \ll 1$ will the contribution from the internal motions be negligible. Lacking such ultra-small-angle resolutions in conventional light-scattering apparatus, however, it becomes crucial to be able to simultaneously solve the dynamics associated with the center-of-mass diffusion and interior segmental relaxations. For a broadly polydisperse system, the situation worsens as these two types of motions for aggregate clusters of considerably varying size become highly entangled. Therefore, there is an imperative need to develop a plausible dynamic structure factor that can be utilized to cope with this central challenge in DLS experiment on aggregated polymer solutions. By extending Pecora's formula as introduced above, we propose a general, self-consistent formulation for solution systems consisting of polymer aggregates with, in principle, arbitrary form factors:

$$|g^{(1)}(q,t,x)| = [P_0(x)/P(x)]\exp(-D_Gq^2t) + [1 - P_0(x)/P(x)]\exp[-(D_Gq^2 + 2/\tau_c)t] \quad (2)$$

At present, the results for Gaussian chains are utilized for the partitioning: $P(x) = \sum_{N=0}^{\infty}P_N(x) = 2/x^2(e^x - 1 + x)$ and $P_0(x) = (\pi/x)\exp(-x/6)[\mathrm{erf}(x^{1/2}/2)]^2$. The central idea is that while the first term on the right side of eq 2 represents the major contribution from center-of-mass diffusion of an individual aggregate species, the second lumps associated internal motions into a single relaxation mode that is independent of q. The major assumption, then, will be that for aggregate species assuming a form other than the Gaussian coil, the partitioning between these two types of motions remains unchanged. The previous assumption could be a stringent one yet seems indispensable at the moment, given that the dynamics theories on general polymer aggregates remain to be developed.

The prime advantage of this contracted formulation for DLS experiment—which is meant for more general applications beyond dilute solution of isolated polymer chains—is that, in conjunction with eq 1, it provides a practically appealing tool to tackle DLS data on a widely polydisperse system, as we demonstrate later for the renowned case with MEH-PPV solutions. It is further dictated that the single intramolecular relaxation time, τ_c, be estimated from the traditional relation $\tau_c = R_g^2/D_G$, where D_G is related to the hydrodynamic radius R_h through the Stokes−Einstein relation: $D_G = k_BT/6\pi\eta R_h$, with k_B, T, and η being the Boltzmann constant, the absolute temperature, and the viscosity of the dispersion medium, respectively. In this context, self-consistent relationship between the two characteristic radii, i.e., R_g and R_h, may be enforced that further restrains admissible form factor for the particular aggregate species under investigation. As two plausible limiting cases, $R_g/R_h = 1.505$ for Gaussian coil[49] and $R_g/R_h = 0.775$ for rigid sphere are considered. For polymer aggregates assuming an overall isotropic shape, as a DDLS experiment would reveal, the results are expected to fall somewhere in between, and it is among the major objectives of this study to discern which of the two cases offers a more authentic description for bulk aggregate clusters in MEH-PPV solutions. Though not attempted in this work, the specific value extracted for R_g/R_h in a combined DLS/SLS experiment may be iterated in eqs 1 and 2 until convergence is warranted. It is, in fact, from this perspective that the proposed formula, eq 2, may be deemed self-consistent.

In the following, the hydrodynamic radii, R_h, of individual aggregate species are treated as the only floating parameter, by assuming either Gaussian coil or solid sphere as the test form factor in analyzing the DLS data on MEH-PPV solutions. The presumed topology of the polymer aggregates is later evaluated against the companion SLS data, where the form factor or R_g may be independently resolved. In this way, we show that self-consistency can be warranted, allowing an unequivocal determination of the morphologies and detailed size distributions of the sample solutions. The attributes of internal segmental dynamics of bulk aggregate clusters can also be unraveled to some extent.

For a unified treatment of both DLS and SLS data, we fit $|g^{(1)}(q,t)|$ with a linear combination of transformed functions in solving the intensity-weighted distribution $G_i(R_h)$ in eq 1. In this "indirect transformation method", the distribution is described by a series of cubic B splines $\varphi_i(R)$ in a range delimited by R_{min} and R_{max}: $G(R) = \sum_{i=1}^{N_s}c_i\varphi_i(R)$, where N_s is the number of cubic B splines used, and the optimum choice of N_s was found to be 15 for analyzing the present DLS and SLS data. Specifically, the same number of modes—equally spaced in logarithmic scale—was utilized to capture the wide size distribution of aggregate species in MEH-PPV solutions. Using simplex optimizations to minimize the objective function of the fit, one can determine unequivocally the coefficient c_i and, hence, the full distribution $G(R)$ in both experiments. Two constraints added to reduce the number of feasible solutions are $0 \le c_i \le 1$ and $\sum_{i=1}^{N_s}c_i = 1$.

On the other hand, the DLS curves may further be characterized by the initial decay rate, defined as $\Gamma_q^{(0)} = \partial/\partial t\,\ln|g^{(1)}(q,t)|\big|_{t=0}$.[50] For instance, the asymptote of $\Gamma_q^{(0)}$ at large x is given by $\Gamma_q^{(0)} = 0.0625k_BTq^3/\eta$ in the Zimm model for theta solvents.[51] For polymer aggregate clusters, the behavior is curious and worth pursuing. In this study, $\Gamma_q^{(0)}$ is approximated

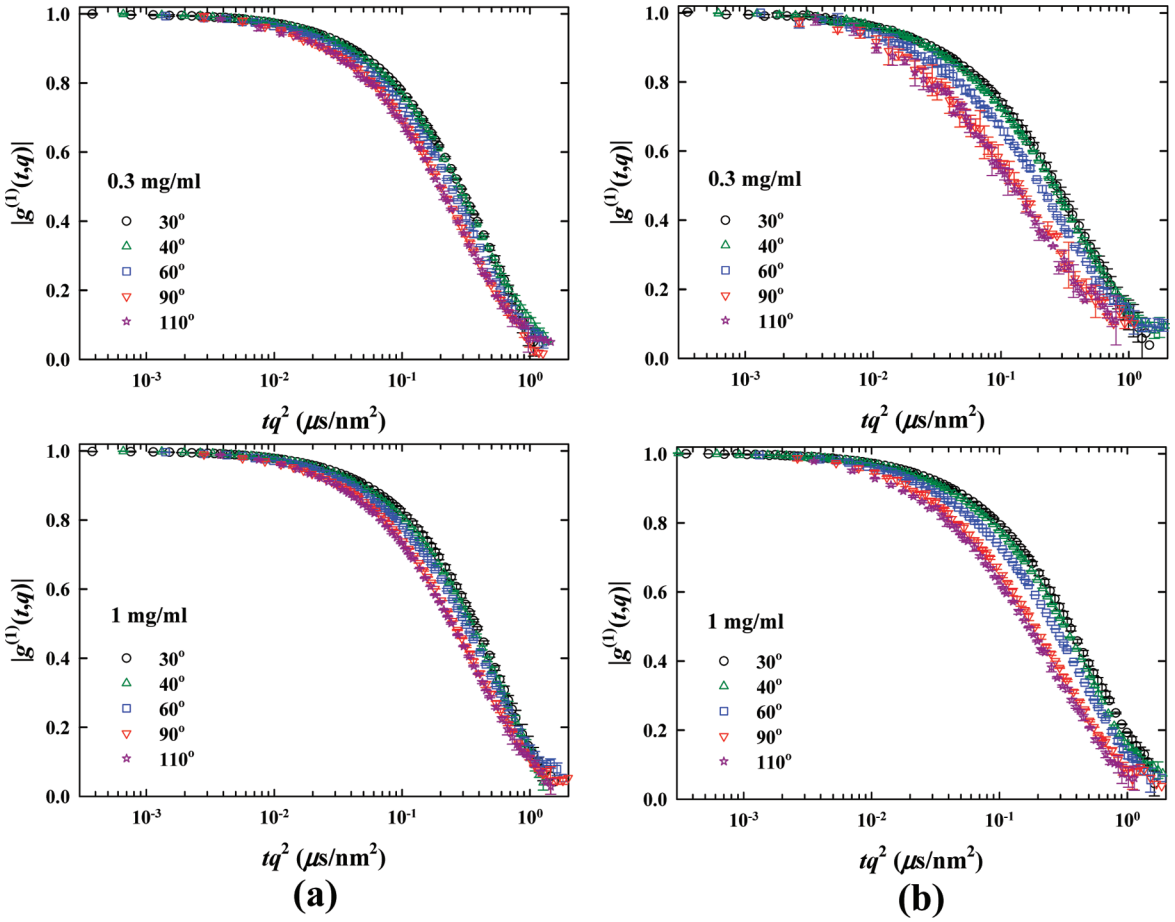

Figure 2. Scattering vector dependences of field autocorrelation function of MEH-PPV in (a) toluene and (b) chloroform over a range of scattering angles for the cases of 0.3 and 1 mg/mL, respectively, where the delay time (t) has been rescaled with q^2.

by the first cumulant $\langle\Gamma\rangle$ ($=\int_0^\infty G(\Gamma)\Gamma\,d\Gamma$)[42,52−54] and is analyzed to gain insight into the internal dynamics of bulk aggregate species in MEH-PPV solutions.

2.4. Static Light Scattering. In SLS experiments, the time-average scattering intensity of the solution, I_{solu}, was corrected for the solvent scattering intensity, I_{solv}, and later converted into the Rayleigh ratio, R_θ, via the relation $R_\theta = (I_{solu} - I_{solv})/I_{tol}(n_{solv}/n_{tol})^2 R_{tol}$,[55] where n_{solv} and n_{tol} denote the refractive indices of solvent and toluene (serving as a reference), respectively, and I_{tol} denotes the scattering intensity of toluene. The Rayleigh ratio of toluene R_{tol} at 633 nm was taken to be 13.59×10^{-6} cm^{-1}.[56]

At $30° \le \theta \le 150°$, SLS data generally represent a superposition of scattering intensities from various aggregate species. Thus, the form factor $P(q)$ of a polydisperse system is formulated as

$$P(q) \equiv I(q)/I(0) = \frac{\int_0^\infty G_n(R)\alpha^2(R)P(qR)\,dR}{\int_0^\infty G_n(R)\alpha^2(R)\,dR} \qquad (3)$$

where $G_n(R)$ is the number-weighted distribution of the characteristic size R, $\alpha(R)$ is the polarizability, and $P(qR)$ is the form factor. The polarizability $\alpha(R)$ is proportional to a power γ of R, i.e., $\alpha(R) \propto R^\gamma$.[57] For Gaussian coils, $\gamma = 2$ and $P(x) = 2/x^2(e^x - 1 + x)$; for rigid spheres, $\gamma = 3$ and $P(qR) = [3(\sin qR - qR\cos qR)/(qR)^3]^2$. The distinct scaling laws of the two species provide a good chance that any postulated form factors of MEH-PPV aggregates may be discriminated in SLS experiments, as we show in this work.

3. RESULTS AND DISCUSSION

3.1. Dynamic Structure Factors. Intensity autocorrelation functions $|g^{(2)}(q,t)|$ were collected over a range of scattering angles ($\theta = 30°-110°$) for MEH-PPV in toluene and chloroform, respectively, at various polymer concentrations: 0.1, 0.3, 1, and 3 mg/mL. The aim is to unveil the aggregate morphologies and internal motions in the first place, so that the mean sizes and detailed size distributions may be determined unambiguously. First, we note that the sample solutions were in a "quasi static" state, and only for sufficiently long aging times (days) would the light-scattering data display appreciable nonequilibrium features.[12] For a solution system in which the constituting chains have a great tendency to form interchain aggregates, the previous observation also suggests that the aggregate species in the sample solutions are largely noninteracting within the experimental time scale. A similar conclusion, in fact, may be reached by comparing the size distributions extracted from DLS and SLS experiments, respectively.

Recent computer simulation has revealed that chloroform, which is attractive to the side-chain groups of MEH-PPV, bears a better solvent quality than toluene, which is attractive to the phenyl backbone, although both fall notably below the theta

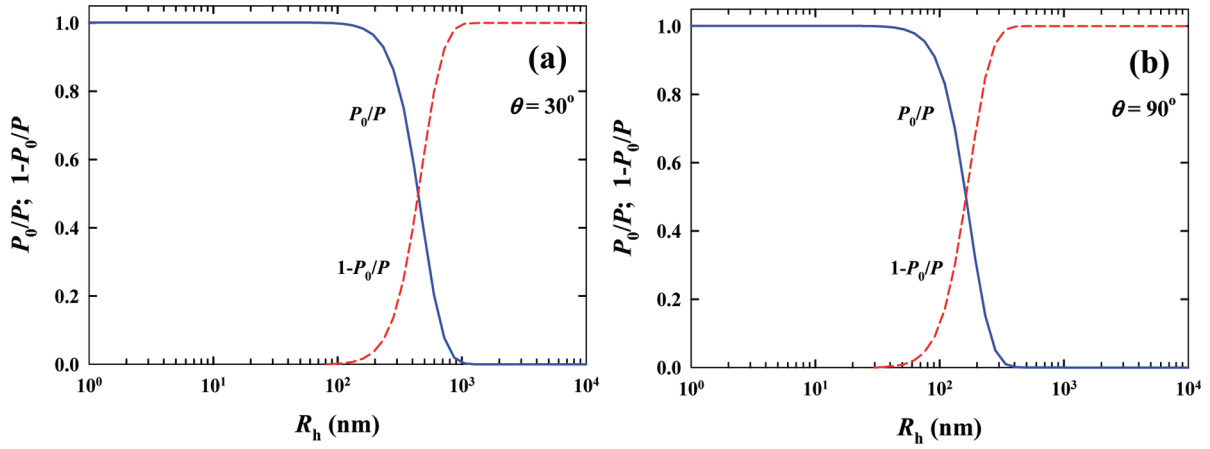

Figure 3. Relative partitioning of translational (solid lines) versus internal (dashed lines) motions as a function of the aggregate size at (a) $\theta = 30°$ and (b) $\theta = 90°$ under the assumption of $R_g/R_h = 0.775$; see also discussion with Figure 4b.

condition.[58] With this essential background, we proceed with the DLS data on individual solvent systems of MEH-PPV. As the results have shown in Figure 2 for some of the sample solutions (0.3 and 1 mg/mL), the field autocorrelation functions $|g^{(1)}(q,t)|$ do not collapse into a single curve after the rescaling of the delay time (t) with q^2, especially for the better solvent, chloroform. Specifically, the acceleration of relaxation with enlarged scattering angle clearly indicates that the contribution from internal segmental motions must be at play. Given that the maximum probe length at the lowest accessible scattering angle (i.e., $1/q \sim 130$ nm at $\theta = 30°$) is not sufficiently larger than the mean hydrodynamic radius $\langle R_h \rangle$ of the aggregate species so resolved, i.e., $q\langle R_h \rangle > 1$, it is not possible under this circumstance to unambiguously resolve the aggregate dynamics and associated material properties without taking into account the interferences between translational diffusion and internal motions. This issue is further pursued below.

Without a priori knowledge of the aggregate structures of MEH-PPV in solution, the DLS curves shown in Figure 2 were analyzed using the formulation proposed in section 2.3 (eqs 1 and 2) for both Gaussian coil and solid sphere as two limiting cases. To simplify the following discussion without loss of generality, we customarily utilize the case with 1 mg/mL for both solvent systems for illustrating purpose. Before the detailed analysis is presented, it is instructive to look at Figure 3 for a prediction of eq 2 on the relative partitioning of the translational (P_0/P) and internal ($1 - P_0/P$) motions, respectively, for the range of aggregate sizes used to fit the DLS data. Depending on the scattering angle, the internal motions of large aggregate species begin to dominate the scattering intensity after the crossover in Figure 3. As expected, the crossover occurs at a smaller aggregate size for a larger scattering angle. Conceptually, the plot states that, while the translational motions have a decaying contribution to the scattering intensity with increasing size, the opposite trend holds for the internal motions. Given that this characteristic feature must hold true in general, the particular form adopted from Gaussian coils for the relative partitioning in eq 2 should be adequate at least qualitatively. It should be borne in mind that the full DLS curve is dictated also by the time-dependent part of eq 2 that is self-consistently determined by the particular form factor assumed, rendering the effect of the partition function less relevant.

For MEH-PPV/toluene solution, the intensity-weighted aggregate distributions $G_i(R_h)$ of the hydrodynamic radius so obtained (at two representative angles 30° and 90°) by assuming two distinct aggregate morphologies are shown in Figure 4, a (coil) and b (sphere), respectively; the corresponding results for MEH-PPV/chloroform solution are given in Figure 5a,b. For comparative purposes, the scattering intensities contributed by the translational and internal motions, respectively, are also plotted. For all the cases investigated, it is evident that the internal motions of MEH-PPV aggregates have a noticeable contribution to the overall scattering intensity, especially at a large scattering angle, $\theta = 90°$. The detailed distributions vary remarkably, however, for different assumptions of the aggregate morphology, and the general trend is in accord with the expectation that internal motions play a more significant role in the case with Gaussian coils than in spherical colloids.

A prompt, though less rigorous, check of the assumptions for two different aggregate morphologies can be made by examining the mean ρ-ratio, denoted as $\langle \rho \rangle$, which is often utilized to characterize structural compactness of a polymer chain or aggregate, where $\langle \rho \rangle = \langle R_g \rangle / \langle R_h \rangle$ with $\langle R_g \rangle$ being the z-average radius of gyration extracted from the Guinier plot of SLS data,[59] which yields a result independent of the form factor, and $\langle R_h \rangle$ the intensity-weighted hydrodynamic radius from DLS data. Thus, the values of $\langle \rho \rangle$ for MEH-PPV/toluene solution at different polymer concentrations were estimated to fall in the range of $0.4 \leq \langle \rho \rangle \leq 0.6$ assuming Gaussian-coil morphology, and in the range of $0.4 \leq \langle \rho \rangle \leq 0.7$ assuming sphere morphology. Given that the theoretical values of $\langle \rho \rangle$ for Gaussian coil and solid sphere are 1.505 and 0.775, respectively, it appears that self-consistency can be better assured by applying the form factor for solid spheres. Similar observations apply to MEH-PPV/chloroform solution, yet with systematically higher values of $\langle \rho \rangle$ (i.e., $0.6 \leq \langle \rho \rangle \leq 0.9$), as might be expected for a better solvent system. Moreover, increasing polymer concentration leads to decreased $\langle \rho \rangle$ in both solvent systems. The significance of $\langle \rho \rangle$ in this study will be revisited later.

It must be reminded that the distributions resolved in Figures 4 and 5 are the result of the superposition of 15 modes that are equally spaced in logarithmic scale, each mode essentially representing an aggregate species falling in a particular size range. These modes contribute to the light-scattering intensity through

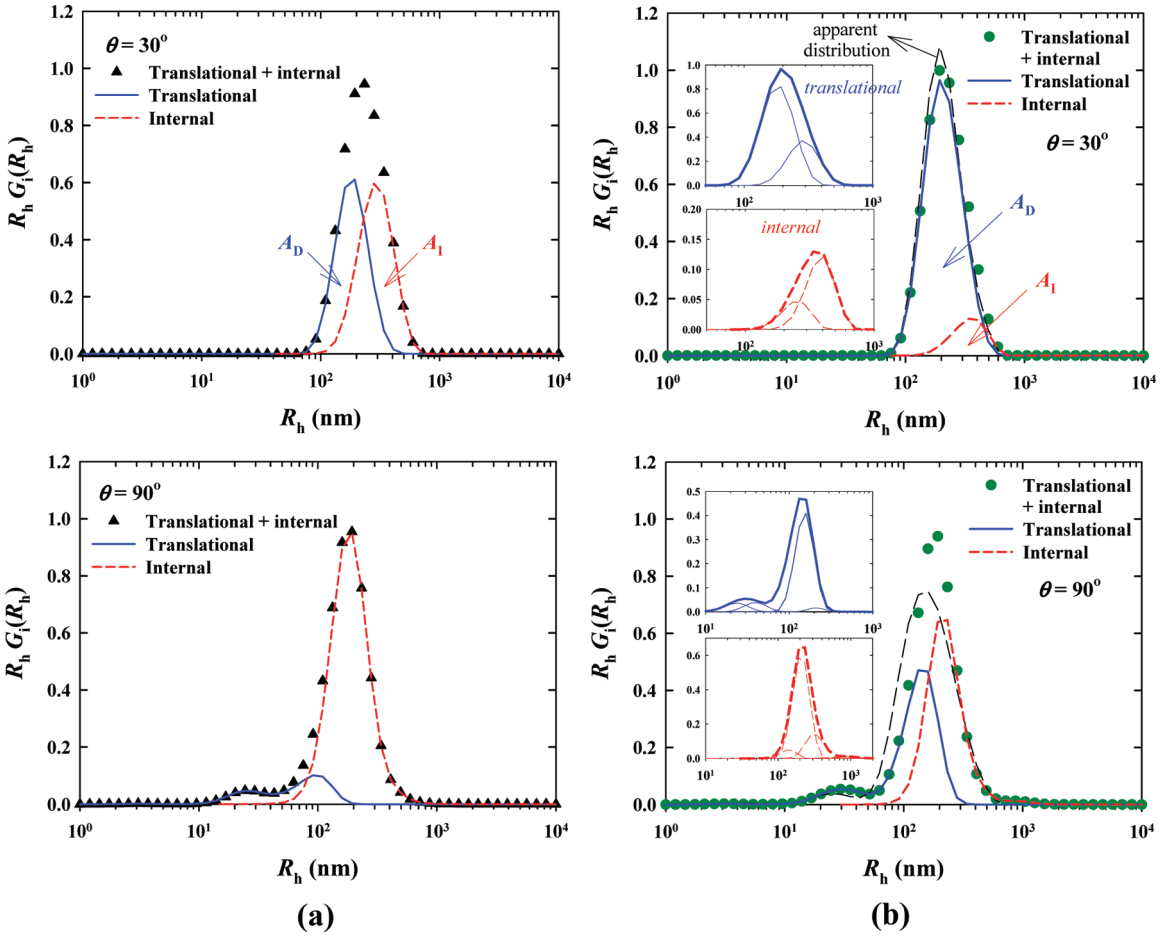

Figure 4. Total intensity-weighted distributions of hydrodynamic radius (translational plus internal motions) retrieved at $\theta = 30°$ and 90°, respectively, for 1 mg/mL MEH-PPV/toluene solution by assuming two different aggregate morphologies: (a) Gaussian coil (▲) and (b) solid sphere (●), where the solid and short-dashed lines represent the scattering intensity contributed by the translational and internal motions, respectively, and the ordinate has been multiplied by R_h in order to make the "visual" areas in each figure better reflect the actual ones on a logarithmic scale. In case (b), the apparent distributions not taking into account the internal motion are also shown for comparison (long-dashed lines), while the inset figures show the actual contribution of each cubic *B* spline that survives the simplex optimization.

the translational motion of the mass center as well as the interior fluctuations, for aggregate species of considerably varying size. For the case considered in Figure 4b and $\theta = 90°$, for instance, it is clear that, in general, the internal motions of large aggregate species contribute a significant amount to the total scattering intensity. In particular, the result shown in Figure 3b suggests that, at this large scattering angle, the internal motions of small aggregate clusters falling in the size range of 10 nm < R_h < 100 nm begin to exhibit nonnegligible contribution to the total scattering intensity. This feature not only explains why a better resolution of small aggregate species may be achieved at a large scattering angle but it also implies that the two distinct contributions of a particular aggregate species facilitate resolving its identity in DLS experiment. In other words, the requirement of concurrently resolving two different motions of each aggregate species has put further restraints in fitting the entire DLS curve.

The central implication that MEH-PPV aggregates in both solvent systems assume a structural feature that deviates substantially from that of a Gaussian coil might be explained by noting that an aggregate cluster "packed" by a large number of random coils lacking pronounced anisotropic local interactions (e.g., hydrogen-bond forces) must, more or less, conform to an isotropic, 3D structure resembling spherical colloids, which bear a fractal exponent of about 4 in contrast with 2 for the Gaussian coil or other species alike. Probably due to the smearing effect of a wide aggregate-size distribution, however, this essential structural feature has often obscured itself in early neutron/X-ray scattering experiments, as we had remarked elsewhere in conjunction with recent computer simulation data on MEH-PPV solutions.[60]

Inspecting the aggregate distributions $G_i(R_h)$ (Figures 4b and 5b) obtained under the assumption of rigid spheres clearly reveals a wide size distribution (10 nm < R_h < 1000 nm) inherent in MEH-PPV solutions. As seen in Figure 4b (and Figure 5b), the position of the main peak is nearly invariant to the scattering angle ($\theta = 30°$ or 90°), which provides a sound justification of eq 2 for essentially all scattering angles. On the other hand, large-angle detections ($\theta \geq 90°$) help better resolve small aggregate species ($R_h \ll 100$ nm) as well as the internal motions, as discussed above, which could become practically invisible at smaller angles. Ideally, using eqs 1 and 2 to fit the DLS data at different angles should yield a nearly identical aggregate distribution, yet in practice they usually possess varied resolutions because of a size-dependent scattering capability at different angles. This observation explains why it is essential to collect

dx.doi.org/10.1021/jp208399z |*J. Phys. Chem. B* 2011, 115, 14369–14380

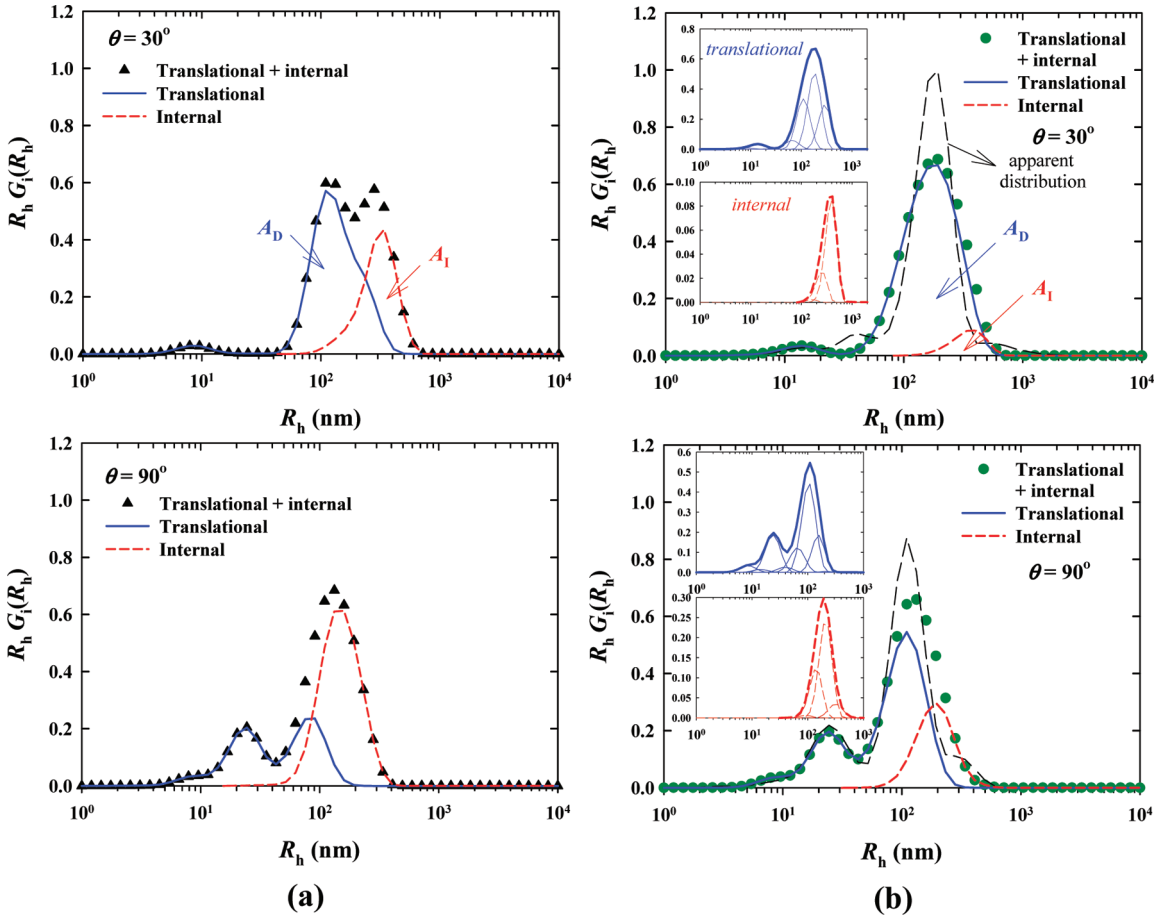

Figure 5. Total intensity-weighted distributions of hydrodynamic radius (translational plus internal motions) retrieved at $\theta = 30°$ and 90°, respectively, for 1 mg/mL MEH-PPV/chloroform solution by assuming two different aggregate morphologies: (a) Gaussian coil (▲) and (b) solid sphere (●), where the solid and short-dashed lines represent the scattering intensity contributed by the translational and internal motions, respectively. In case (b), the apparent distributions not taking into account the internal motion are also shown for comparison (long-dashed lines), while the inset figures show the actual contribution of each cubic *B* spline that survives the simplex optimization.

DLS data at multiple angles, as well as to have in hand a reliable constitutive equation like eq 2, in order to unambiguously resolve the aggregation properties of a widely polydisperse system.

As one "turns off" the contribution from internal motions, i.e., by setting $P(x) = P_0(x)$ in eq 2, and sees how the predicted distribution would be affected, the results should correspond to the usual cases where the particle size distribution was interpreted according to the nominal modes distribution. Thus, the long-dashed lines in Figures 4b and 5b have been obtained by the modes distribution directly extracted from CONTIN.[61] It can be seen that the nominal size distribution may considerably deviate from the actual one that takes into account the interference from internal motions, and the position of the main peak skews as a result at a different scattering angle.

Figure 6 shows the area ratio $A_I/(A_D + A_I)$ denoting the fraction of the scattering intensity (obtained from an integration of the results shown in Figures 4 and 5) from the internal motions for the two solvent systems, where A_D represents the contribution from the mass-center diffusion. As expected, the internal motions come into play at $q\langle R_g\rangle \geq 1$. In general, this ratio for MEH-PPV/toluene solution keeps increasing with increased $q\langle R_g\rangle$, whereas it quickly reaches a plateau for MEH-PPV/chloroform solution at low concentrations. These trends are understandable, considering there is a relatively small amount of MEH-PPV aggregates in chloroform that meet the criterion $qR_g > 1$ and thus contribute much less to the scattering intensity in this high-q regime; only as the concentration is elevated to 3 mg/mL can a ratio as high as ~0.5 be attained at large angles. Overall, as the contribution from the internal motions of MEH-PPV aggregates is concerned, the results shown in Figures 4−6 suggest that both mean aggregate size (or its distribution) and structural compactness matter. For MEH-PPV/toluene solutions, for instance, the former apparently dominates over the latter effect in accounting for a more pronounced contribution from the internal motions.

From a different perspective, we discuss a more detailed analysis of the interior dynamics of large aggregate species. Following the prediction of the Zimm model, for example, the reduced first cumulant $\Gamma_q^{(0)}\eta/q^3k_BT$ as a function of $q\langle R_g\rangle$ has often been employed to fathom the internal dynamics of flexible polymer solutions under the influence of hydrodynamic interactions. Figure 7 shows such relation for MEH-PPV solutions, along with the experimental results on polystyrene/toluene solutions reported earlier.[38] For the poorer-solvent MEH-PPV/toluene solutions, the reduced cumulant begins to exhibit a plateau (q^3 dependence) at relatively large values of $q\langle R_g\rangle$ compared with MEH-PPV/chloroform solutions. In general, this quantity falls substantially below that for polystyrene/toluene

dx.doi.org/10.1021/jp208399z |J. Phys. Chem. B 2011, 115, 14369–14380

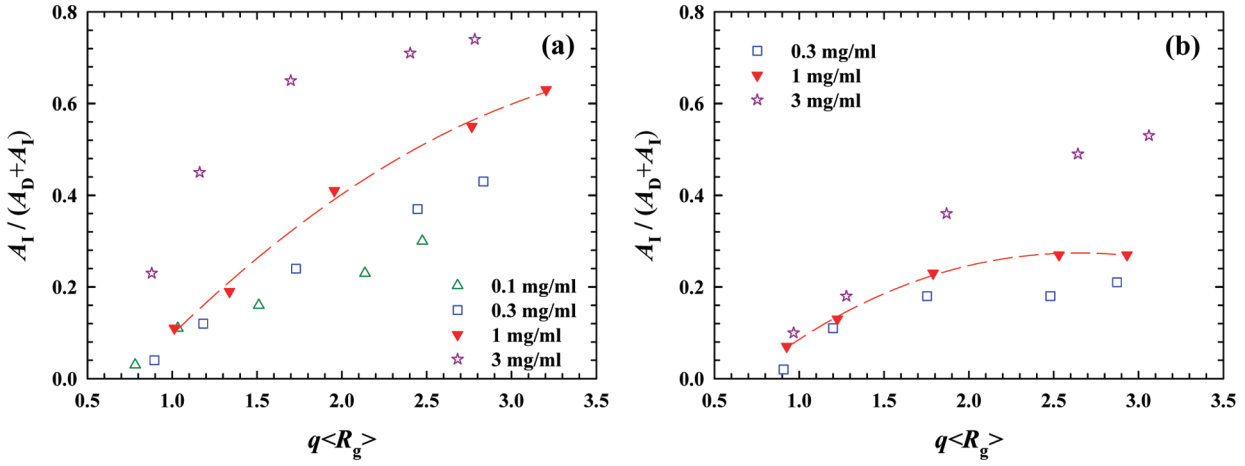

Figure 6. Area ratio $A_I/(A_D + A_I)$ marking the relative contribution of internal motions to the total scattering intensity at different scattering angles for MEH-PPV in (a) toluene and (b) chloroform; lines are used to guide the eyes.

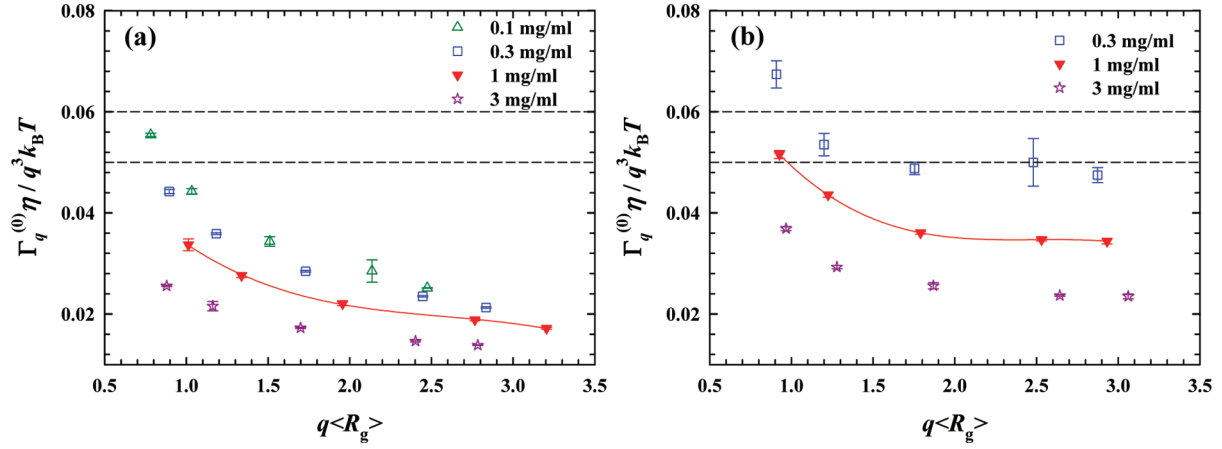

Figure 7. Reduced first cumulant $\Gamma_q^{(0)}\eta/q^3k_BT$ at different scattering angles for MEH-PPV in (a) toluene and (b) chloroform; lines are guide to the eyes. The dashed lines mark the range of experimental values at $q\langle R_g\rangle \gg 1$ for polystyrene/toluene solutions.

solutions, indicating that the internal motions of MEH-PPV aggregates are considerably more suppressed, possibly due to stronger segmental interactions. Moreover, the suppression in internal motions becomes more prominent with decreasing solvent quality or with increasing polymer concentration. Similar trends have been noticed earlier in comparing the responses of PNIPAM linear chains and their microgels, the internal motions of which remain undetectable until at $q\langle R_g\rangle \geq 4$.[44] Evidently, segmental motions within MEH-PPV clusters enjoy a better degree of freedom than for typical polymer gels.

As contrasted with the Zimm model, a free-draining bead–spring model such as the Rouse model predicts that the initial decay rate $\Gamma_q^{(0)}$ at $q\langle R_g\rangle \gg 1$ is controlled by not only the system temperature and solvent viscosity but also the chain dimension, besides a distinct scaling law with the scattering vector, $\Gamma_q^{(0)} = 0.5D_Gq^4R_g^2 \sim q^4$.[53] Thus, the reduced first cumulant, $\Gamma_q^{(0)}/q^4$ is plotted versus $q\langle R_g\rangle$ in Figure 8. It is of interest to note that the data on various concentrations for both solvent systems of MEH-PPV seem to better collapse on the same curve, compared with the results shown in Figure 7. It is curious whether this could be an indication that the interior dynamics of MEH-PPV aggregates are better described within the free-draining limit, as the original formula of Pecora has stood for. Or the agreement was simply a revelation that there exists certain universal relationship dictating the concentration fluctuations within the polymer aggregates, in a form as hinted by the plot shown in Figure 8. In summary, the present DLS analyses suggest that segmental motions within MEH-PPV aggregates are much more hampered than in the counterpart nonaggregated polymer solutions, yet they still enjoy certain flexibility not permissible for typical polymer microgels. In view of the asymptotical behavior at high q, none of the existing theories within the bead–spring picture for dilute solution of isolated polymer chains seem to readily capture the data, which exhibit a persistent q-dependence up to the high-q regime.

For its ability to resolve optically anisotropic particulate species, depolarized dynamic light scattering (DDLS) has also been performed for some of the MEH-PPV sample solutions, and the results were found to be VH-inactive, suggesting that the aggregate species assume a virtually isotropic shape. This observation is expectable for van der Waals forces-driven polymer associates; it also lends support to the colloid-like sphere assumption in interpreting the DLS data.

3.2. Static Light Scattering Form Factors. As implied by the DLS data above, it is usually essential to consult the SLS data in order to confirm the basic assumptions made on the form factor. In contrast with the DLS analysis which resolves the feature of

dx.doi.org/10.1021/jp208399z |J. Phys. Chem. B 2011, 115, 14369–14380

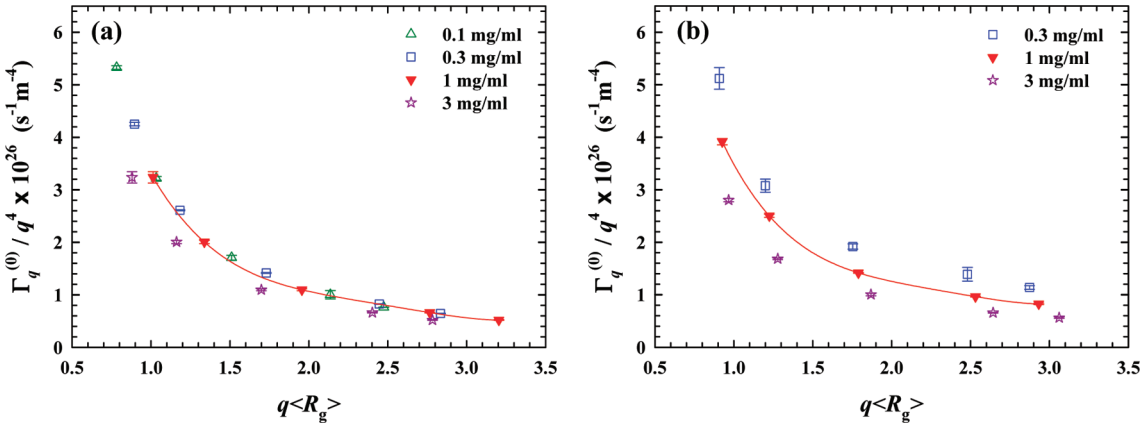

Figure 8. Reduced first cumulant $\Gamma_q^{(0)}/q^4$ at different scattering angles for MEH-PPV in (a) toluene and (b) chloroform; lines are guide to the eyes.

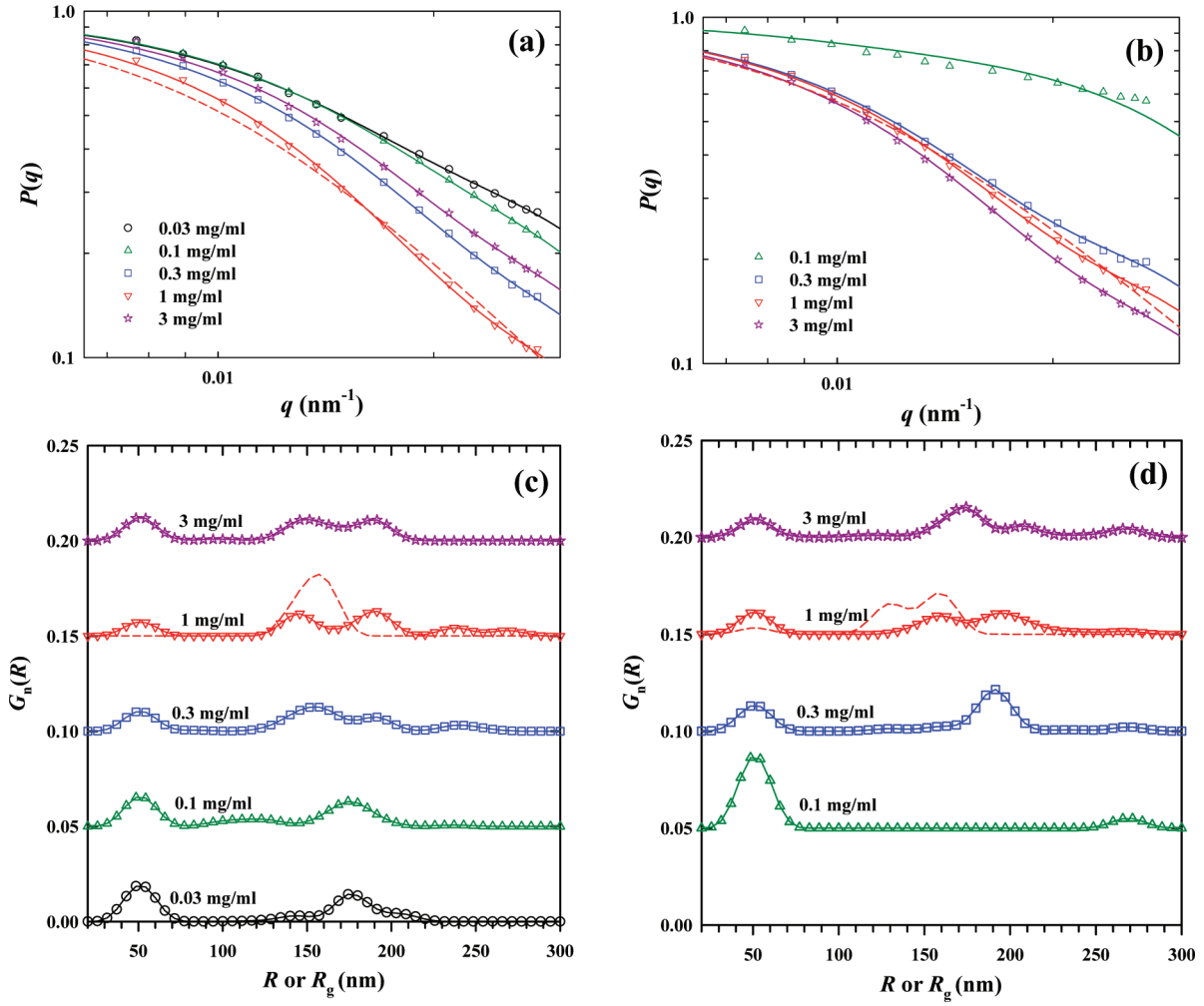

Figure 9. Experimental form factors for MEH-PPV in (a) toluene and (b) chloroform at various concentrations, where the solid lines are fits to the data using eq 3 with the form factor of sphere; also shown are the predictions for Gaussian coil, dashed lines, for the illustrating case of 1 mg/mL. The corresponding number-weighted size distributions are shown in (c) and (d), respectively.

hydrodynamic radius, R_h, the corresponding SLS data are good at extracting the properties of the radius of gyration, R_g, through the form-factor analysis for noninteracting solution systems. In Figure 9a,b, the experimental form factors, $P(q)$, in both solvent systems provide compelling evidence that the data can be well described by the form factor for polydisperse spheres (solid lines; eq 3), but not for Gaussian coils. An illustrating example is provided for the case of 1 mg/mL, shown by the dashed lines in

dx.doi.org/10.1021/jp208399z |J. Phys. Chem. B 2011, 115, 14369–14380

Table 1. Summary of the Aggregate Properties of MEH-PPV in Two Different Solvent Systems

c (mg/mL)	$\langle R_h \rangle$ (nm)	$\langle R_g \rangle$ (nm)	$\langle \rho \rangle$	$\langle M \rangle_{w,app}$ (g/mol)	$\langle N_{agg} \rangle$
		MEH-PPV/Toluene			
0.03	–	101	–	1.2×10^6	12
0.1	152	101	0.7	4.2×10^6	42
0.3	175	116	0.7	7.8×10^6	78
1	233	131	0.6	9.9×10^6	99
3	316	114	0.4	3.9×10^6	39
		MEH-PPV/Chloroform			
0.1	–	73	–	–	–
0.3	142	122	0.9	0.9×10^5	9
1	192	124	0.7	1.7×10^6	17
3	231	130	0.6	1.5×10^6	15

Figure 9, where capturing the experimental data was noted to be beyond the reach of simplex optimizations during the curve fitting—clearly indicative of the inappropriateness of the form factor assumed. It is intriguing to notice that, even for a widely polydisperse system, the SLS data remain quite discriminative to the fundamental structure of bulk aggregate species. In summary, assuming a noninteracting condition which should apply to most of the sample solutions investigated, the SLS data provide a firm confirmation to the sphere-like form factor for the aggregate clusters in MEH-PPV solutions, as supported by recent computer simulations.[60]

Indeed, comparing the aggregate distributions resolved in Figures 4b and 9c, for instance, by DLS and SLS analyses, respectively, reveals several unanimous features for MEH-PPV/toluene solutions. First, the two main peaks in Figure 9c having radii larger than 100 nm may be associated with the primary, yet broader, peak in Figure 4b. A similar correspondence can be noted for MEH-PPV/chloroform solutions as well (cf., Figures 5b and 9d). Moreover, the aggregate species with radii below 100 nm, which manifest themselves only at large angles in DLS experiment, were readily resolved by SLS as well. In contrast, these small aggregate species would be largely missing if the form factor of Gaussian coil is assumed instead (see, for instance, dashed lines in Figure 9c,d).

As has been noted earlier, the mean particle sizes obtained from DLS and SLS analyses, respectively, i.e., $\langle R_h \rangle$ and $\langle R_g \rangle$, are often utilized to infer the structural compactness through the ratio $\langle \rho \rangle = \langle R_g \rangle / \langle R_h \rangle$, and a smaller value of $\langle \rho \rangle$ has typically been assigned to a more compact structure. The results for all sample solutions are tabulated in Table 1. To our surprise, the results obtained for MEH-PPV solutions occasionally fall even below the theoretical value for solid spheres, i.e., $\langle \rho \rangle = 0.775$, while derailing markedly from that for Gaussian coils, $\langle \rho \rangle = 1.505$. As an independent appraisal, therefore, we have also evaluated the aggregate density ρ_{agg} using the expression $\rho_{agg} = \langle M \rangle_{w,app} / (N_A 4\pi \langle R_g \rangle^3/3)$, where the apparent weight-averaged molecular weight $\langle M \rangle_{w,app}$ of the aggregates is estimated by the relation $\langle M \rangle_{w,app} \cong R_{VV}(q=0)/Kc$, with $R_{VV}(q=0)$ and K being the (extrapolated) Rayleigh ratio at $q = 0$ and the optical constant, respectively. Intriguingly, we found that ρ_{agg} for MEH-PPV/toluene solutions is not much different from that of polystyrene/toluene solutions at 25 °C, i.e., $\rho_{PS} \cong 0.002$ g/cm^3.[62] Thus, aside from a possible influence of polydispersity on this particular ratio, it seems that the apparently low values of $\langle \rho \rangle$ for MEH-PPV solutions might not be interpreted here as suggesting a rather compact aggregate structure.

For aggregate clusters formed by loosely connected, independent chains, like the case with MEH-PPV for which weak van der Waals forces dominate the segmental interactions in solution state, it is possible that the center-of-mass diffusivity, which has been utilized to define R_h, may not precisely correlate with the geometric one such as R_g. Consider the following, somewhat extreme, case: when a few loosely connected chains form a small aggregate species, the motions of individual chains remain largely independent and randomized and, hence, it is difficult for the aggregate to develop definite diffusive movement as a whole. In turn, the seemingly sluggish dynamics of the aggregate would yield an apparently large value of R_h. A similar reason, perhaps, might explain a relatively enlarged $\langle R_h \rangle$ from DLS measurements in comparison with $\langle R_g \rangle$, which may be resolved unequivocally in SLS experiment—by the Guinier plot or a detailed form-factor analysis. In summary, given the yet-uncertain attributes of the dynamic feature of polymer aggregates in various solution systems, the conventional wisdom for utilizing the relation between these two characteristic radii to infer the structural compactness should be prudently confirmed.

Finally, with $\langle M \rangle_{w,app}$ available from the above analysis, the mean aggregation number $\langle N_{agg} \rangle$ can be known for each MEH-PPV solution system, as also provided in Table 1. This quantity has been evaluated using the relation $\langle M \rangle_{w,app}/\langle M \rangle_n$, with $\langle M \rangle_n$ being the reported number average molecular weight for the MEH-PPV sample used in this study. Considering the difficulties in precisely determining the real polymer weight, as well as the reported polydispersity (~5) associated with the sample, the results given in Table 1 should only hint at the approximate aggregation number in typical MEH-PPV solutions. In this context, it is of interest to note that the present experimental estimation agrees well with recent computer simulations, which suggest that while aggregate clusters consisting of more than 50 chains are pervasively observable in MEH-PPV/toluene solution, only much looser aggregate clusters composed of a few tens of chains seem to be viable in MEH-PPV/chloroform solution.[60]

4. CONCLUSION

We proposed a self-consistent formulation for analyzing the dynamic structure factor of aggregate species in dilute solutions of a standard conjugated polymer, where a wide size distribution and unknown aggregate morphology have posed stringent challenges for conventional light-scattering analyses. The essential feature of this new formulation lies in that only readily accessible angular detections are required, and DLS data on two different angles (e.g., 30° and 90°) usually suffice this purpose. The formulation has been inspired by an existing theory on free-draining bead−spring chains with internal fluctuations yet is meant for more general applications, allowing various candidate form factors to be self-consistently tested in combined DLS and SLS measurements. Fair self-consistency in the resolved form factor and aggregate size distribution in both light-scattering measurements of MEH-PPV solutions clearly lends support to the proposed formulation for its capability of tackling solution systems with simultaneously a wide size distribution and unknown structural features.

Specifically, for MEH-PPV/chloroform and MEH-PPV/toluene solutions over a range of concentrations, $c = 0.1-3$ mg/mL, both form-factor analysis of SLS data and extracted

values for $\langle\rho\rangle = \langle R_g\rangle/\langle R_h\rangle$ (around 0.7) in combined DLS/SLS measurements unanimously support the *sphere* morphology of bulk aggregate clusters. This central conclusion differs from early neutron/X-ray scattering studies inferring certain 2D fractal structures for the aggregation network, which might be blamed for the effects of polydispersity as well as a limited range of probe length scales (typically, <100 nm). Detailed analyses of the interior dynamics of the aggregate clusters revealed that segmental motions within are generally more suppressed than for nonaggregated polymer solutions, yet remain sufficiently flexible compared with typical polymer microgels. Further, the observed scaling behavior at $q\langle R_g\rangle > 1$ cannot be readily captured by existing bead−spring theories for dilute solution. Another salient feature was that the structural compactness inferred from the ratio $\langle\rho\rangle$ deviates notably from a direct estimate of the monomer density, prompting a rethinking of data interpretation for polymer aggregate clusters based on this conventional wisdom.

Accordingly, we were able to report several first-revealed properties of MEH-PPV solutions on the aggregate morphology, the size distribution (and mean size), mean aggregation number, and interior segmental dynamics, which serve as valuable information for linking solution properties with those for dried thin films—a quest that has since been pursued yet for long remained at an empirical level. In future perspective, the current formulation should benefit from an improved knowledge on the interior dynamics of polymer aggregates, through new theories or commissioned computer simulations.

AUTHOR INFORMATION

Corresponding Author

*E-mail: chmcch@ccu.edu.tw. Fax: +886-5-2721206.

ACKNOWLEDGMENT

This work is supported by the National Science Council of ROC under grant no. NSC100-2120-M007-009.

REFERENCES

(1) Burroughes, J. H.; Bradley, D. D. C.; Brown, A. R.; Marks, R. N.; Mackay, K.; Friend, R. H.; Burns, P. L.; Holmes, A. B. *Nature* **1990**, *347*, 539.

(2) Kraft, A.; Grimsdale, A. C.; Holmes, A. B. *Angew. Chem. Int. Ed.* **1998**, *37*, 402.

(3) Yu, G.; Gao, J.; Hummelen, J. C.; Wudl, F.; Heeger, A. J. *Science* **1995**, *270*, 1789.

(4) Brabec, C. J.; Sariciftci, N. S.; Hummelen, J. C. *Adv. Funct. Mater.* **2001**, *11*, 15.

(5) Halls, J. J. M.; Walsh, C. A.; Greenham, N. C.; Marseglia, E. A.; Friend, R. H.; Moratti, S. C.; Holmes, A. B. *Nature* **1995**, *376*, 498.

(6) Nguyen, T.-Q.; Doan, V.; Schwartz, B. J. *J. Chem. Phys.* **1999**, *110*, 4068.

(7) Chen, S. H.; Su, A. C.; Huang, Y. F.; Su, C. H.; Peng, G. Y.; Chen, S. A. *Macromolecules* **2002**, *35*, 4229.

(8) Collison, C. J.; Rothberg, L. J.; Treemaneekarn, V.; Li, Y. *Macromolecules* **2001**, *34*, 2346.

(9) Shi, Y.; Liu, J.; Yang, Y. *J. Appl. Phys.* **2000**, *87*, 4254.

(10) Mahfoud, A.; Sarangan, A.; Nelson, T. R.; Blubaugh, E. A. *J. Lumin.* **2006**, *118*, 123.

(11) Quan, S.; Teng, F.; Xu, Z.; Qian, L.; Hou, Y.; Wang, Y.; Xu, X. *Eur. Polym. J.* **2006**, *42*, 228.

(12) Chen, S. H.; Su, A. C.; Chang, C. S.; Chen, H. L.; Ho, D. L.; Tsao, C. S.; Peng, K. Y.; Chen, S. A. *Langmuir* **2004**, *20*, 8909.

(13) Ou-Yang, W.-C.; Chang, C.-S.; Chen, H.-L.; Tsao, C.-S.; Peng, K.-Y.; Chen, S.-A.; Han, C. C. *Phys. Rev. E* **2005**, *72*, 031802.

(14) Li, Y.-C.; Chen, C.-Y.; Chang, Y.-X.; Chuang, P.-Y.; Chen, J.-H.; Chen, H.-L.; Hsu, C.-S.; Ivanov, V. A.; Khalatur, P. G.; Chen, S.-A. *Langmuir* **2009**, *25*, 4668.

(15) Choudhury, P. K.; Bagchi, D.; Menon, R. *J. Phys.: Condens. Matter* **2009**, *21*, 195801.

(16) Zhang, G.; Wu, C. *Adv. Polym. Sci.* **2006**, *195*, 101.

(17) Ye, J.; Xu, J.; Hu, J.; Wang, X.; Zhang, G.; Liu, S.; Wu, C. *Macromolecules* **2008**, *41*, 4416.

(18) Kubota, K.; Fujishige, S.; Ando, I. *J. Phys. Chem.* **1990**, *94*, 5154.

(19) Kujawa, P.; Aseyev, V.; Tenhu, H.; Winnik, F. M. *Macromolecules* **2006**, *39*, 7686.

(20) Kjoniksen, A.-L.; Zhu, K.; Pamies, R.; Nystrom, B. *J. Phys. Chem. B* **2008**, *112*, 3294.

(21) Petekidis, G.; Vlassopoulos, D.; Fytas, G.; Kountourakis, N.; Kumar, S. *Macromolecules* **1997**, *30*, 919.

(22) Laflèche, F.; Durand, D.; Nicolai, T. *Macromolecules* **2003**, *36*, 1331.

(23) Matsuda, Y.; Sato, T.; Oishi, Y.; Watanabe, H. *J. Polym. Sci., Part B: Polym. Phys.* **2005**, *43*, 1401.

(24) Liu, S.; Armes, S. P. *Langmuir* **2003**, *19*, 4432.

(25) Otsuka, I.; Fuchise, K.; Halila, S.; Fort, S. b.; Aissou, K.; Pignot-Paintrand, I.; Chen, Y.; Narumi, A.; Kakuchi, T.; Borsali, R. *Langmuir* **2009**, *26*, 2325.

(26) Loos, K.; Böker, A.; Zettl, H.; Zhang, M.; Krausch, G.; Müller, A. H. E. *Macromolecules* **2005**, *38*, 873.

(27) Demeter, J.; Mormann, W.; Schmidt, J.; Burchard, W. *Macromolecules* **2003**, *36*, 5297.

(28) Yusa, S.-i.; Kamachi, M.; Morishima, Y. *Langmuir* **1998**, *14*, 6059.

(29) Karayianni, M.; Mountrichas, G.; Pispas, S. *J. Phys. Chem. B* **2010**, *114*, 10748.

(30) Hou, Y.; Yu, C.; Liu, G.; Ngai, T.; Zhang, G. *J. Phys. Chem. B* **2010**, *114*, 3799.

(31) Dai, Z.; Ngai, T.; Wu, C. *Soft Matter* **2011**, *7*, 4111.

(32) Yang, D.; Zhang, J. Z.; Fu, S.; Xue, Y.; Hu, J. *Colloids Surf. A* **2010**, *353*, 197.

(33) Ehrl, L.; Soos, M.; Lattuada, M. *J. Phys. Chem. B* **2009**, *113*, 10587.

(34) Yuan, L.; Tang, Q.; Yang, D.; Zhang, J. Z.; Zhang, F.; Hu, J. *J. Phys. Chem. C* **2011**, *115*, 9926.

(35) de Gans, B. J.; Wiegand, S.; Zubarev, E. R.; Stupp, I. *J. Phys. Chem. B* **2002**, *106*, 9730.

(36) Sedlák, M. *J. Phys. Chem. B* **2006**, *110*, 4329.

(37) Sedlák, M. *J. Phys. Chem. B* **2006**, *110*, 4339.

(38) Wu, C.; Chan, K. K.; Xia, K.-Q. *Macromolecules* **1995**, *28*, 1032.

(39) Huang, W.-N.; Frederick, J. E. *Macromolecules* **1974**, *7*, 34.

(40) Dai, Z.; Wu, C. *Macromolecules* **2010**, *43*, 10064.

(41) Tsunashima, Y.; Nemoto, N.; Kurata, M. *Macromolecules* **1983**, *16*, 584.

(42) Chu, B.; Wang, Z.; Yu, J. *Macromolecules* **1991**, *24*, 6832.

(43) Nicolai, T.; Brown, W.; Johnsen, R. *Macromolecules* **1989**, *22*, 2795.

(44) Wu, C.; Zhou, S. *Macromolecules* **1996**, *29*, 1574.

(45) Siegert, A. J. F. *MIT Radiation Lab. Report* 1943, No. 475.

(46) Berne, B. J.; Pecora, R. *Dynamic Light Scattering*; Dover: New York, 2000.

(47) Pecora, R. In *Dynamic Light Scattering: Applications of Photon Correlation Spectroscopy*; Pecora, R., Ed.; Plenum Press: New York, 1985.

(48) Pecora, R. *J. Chem. Phys.* **1968**, *49*, 1032.

(49) Schärtl, W. *Light Scattering from Polymer Solutions and Nanoparticle Dispersions*; Springer: Berlin, 2007.

(50) Doi, M. *Introduction to Polymer Physics*; Oxford University Press: New York, 1995.

(51) Doi, M.; Edwards, S. F. *The Theory of Polymer Dynamics*; Oxford University Press: New York, 1986.

(52) Han, C. C.; Akcasu, A. Z. *Macromolecules* **1981**, *14*, 1080.

(53) Teraoka, I. *Polymer Solutions*; Oxford University Press: New York, 2002.
(54) Sorlie, S. S.; Pecora, R. *Macromolecules* **1988**, *21*, 1437.
(55) Chu, B. *Laser Light Scattering: Basic Principles and Practice*; Dover: New York, 2007.
(56) Pike, E. R.; Pomeroy, W. R. M.; Vaughan, J. M. *J. Chem. Phys.* **1975**, *62*, 3188.
(57) Aragon, S. R.; Pecora, R. *J. Chem. Phys.* **1976**, *64*, 2395.
(58) Lee, C. K.; Hua, C. C.; Chen, S. A. *J. Phys. Chem. B* **2008**, *112*, 11479.
(59) Roe, R. J. *Methods of X-ray and Neutron Scattering in Polymer Science*; Oxford University Press: New York, 2000.
(60) Shie, S. C.; Lee, C. K.; Hua, C. C.; Chen, S. A. *Macromol. Theory Simul.* **2010**, *19*, 179.
(61) Provencher, S. W. *Comput. Phys. Commun.* **1982**, *27*, 229.
(62) Min, G.; Savin, D.; Gu, Z.; Patterson, G. D.; Kim, S. H.; Ramsay, D. J.; Fishman, D.; Ivanov, I.; Sheina, E.; Slaby, E.; Oliver, J. *Int. J. Polym. Anal. Charact.* **2003**, *8*, 187.